INTEGRATING MULTIPLE NONLINEAR ESTIMATORS INTO HYPERSPECTRAL UNMIXING

Andrea Marinoni[1], *Javier Plaza*[2], *Antonio Plaza*[2] *and Paolo Gamba*[1]

[1]Dipartimento di Ingegneria Industriale e dell'Informazione, Università degli Studi di Pavia, Pavia, Italy.
E-mail: {andrea.marinoni, paolo.gamba}@unipv.it
[2]Hyperspectral Computing Laboratory, University of Extremadura, Cáceres, Spain.
E-mail: {jplaza, aplaza}@unex.es

ABSTRACT

Linear spectral unmixing has been widely used for hyperspectral data interpretation. However, there is a need for nonlinear unmixing methods that can model more complex geometries without the need to resort to prior knowledge about the objects in the scene. In this paper, we present a novel strategy for nonlinear spectral unmixing which combines polytope decomposition (POD) with artificial neural network (ANN)-based learning. Even if no ground-truth information is available, the ANN can still efficiently estimate the order of the nonlinearity involved in the problem and enhance the capacity of the POD method to deliver unmixing performance for a wider range of nonlinearities. The proposed method has been evaluated using both simulated and real scenes, providing promising results.

Index Terms— Nonlinear hyperspectral unmixing, artificial neural networks (ANNs), polytope decomposition (POD).

1. INTRODUCTION

Spectral unmixing is an important task for remotely sensed hyperspectral data exploitation [1, 2]. Linear spectral unmixing [3] has been the most popular approach in practice. This model aims at decomposing the original hyperspectral scene into a collection of spectrally pure components (called *endmembers* [4] in spectral unmixing jargon) and their corresponding fractional abundances at a pixel level. The linear mixture model holds true when the mixing scale is macroscopic and the incident light interacts with just one material, as is the case in checkerboard type scenes [1]. This model has been widely used mainly due to its simplicity as an acceptable approximation for the light scattering in many real scenarios, and also to the fact that, under suitable conditions of the data set, this model yields well-posed inverse problems. However, the main limitation of the linear mixture model lies in its inability to deal with more complex (and realistic) geometries [5].

Research on nonlinear spectral unmixing can be considered yet immature as compared to linear spectral unmixing. To avoid the complex physical models, usually simpler strategies are applied using data-driven but physics-inspired models, such as the bilinear [1] and Hapke's models [6]. The bilinear model is valid when the scene can be partitioned in successive layers with similar scattering properties. Kernel-based methods have also been explored as an alternative to handle the problem of intimate mixtures. Linear kernels, radial-basis functions, polynomial, and physics-based kernels were proposed [7]. To cope with both scattering and intimate mixture problems simultaneously, artificial neural network (ANN) technologies have been recently proposed [8], where training samples are used to learn nonlinearities (see [9] and references therein). Polynomial functions can be applied as well to model the nonlinearities [10]. A common aspect of the aforementioned methods is that they require prior knowledge. Fully unsupervised nonlinear unmixing methods have only very recently been explored. One possibility is to work directly on the nonlinear data manifold on which it can be shown that the concepts of convex geometry still hold. Geodesic distances can be calculated on manifolds induced by nonlinear models [11].

In this work, we present a novel strategy for nonlinear spectral unmixing which combines polytope decomposition (POD) with ANN-based learning. Previous studies [12] have shown that the POD method is able to deliver very good performance in terms of reconstruction error over scenes where no ground-truth is previously available and the nonlinearity can be described by means of polynomials. It has been observed, however, that if the nonlinearity is non-polynomial (e.g., sinusoidal), the POD method does not show good performance in spectral unmixing. Further, the aforementioned method can not estimate the order of the nonlinearity itself, an aspect that can lead to lower unmixing performance and/or overfitting. These issues can be addressed by using supervised ANNs which are able to deliver unmixing performance for a wider range of nonlinearities. Even if no ground-truth information is available, the ANN can still efficiently estimate the order of the nonlinearity involved in the problem, thus enhancing the capacity of the POD method. As a result, it is possible to set up a framework for unsupervised hyperspectral unmixing that makes use of the POD method in order to achieve the nonlinear coefficients and to efficiently reconstruct the image from the extracted endmembers.

The remainder of the paper is organized as follows. Section 2 describes the POD and ANN methods used in this work to develop the proposed approach. Section 3 presents an experimental validation of the proposed approach. Section 4 concludes the paper with some remarks and hints at plausible future research lines.

2. METHODS

Fig. 1 shows a flowchart of the proposed approach, which is made up of the combination of POD and ANN techniques applied to the original hyperspectral image after obtaining a set of endmembers using an endmember extraction algorithm (EEA). In this section we describe the aforementioned methods in more details.

2.1. Polytope decomposition (POD)

Let $\underline{s} = [s_i]_{i=1,\dots,n}$, $s_i \in [0,1]$ be the n-band spectral signature of one pixel in a hyperspectral image. Let us assume that the sig-

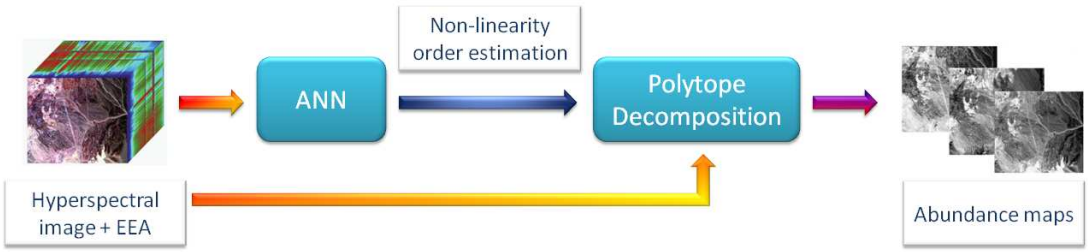

Fig. 1. Scheme of the proposed framework for nonlinear spectral unmixing.

nature $\underline{s}$ is a nonlinear combination of r endmembers $\underline{e^{(j)}}$, being $j = 1, \ldots, r$. Hence, it is possible to write $s_i \; \forall i \in \{1, \ldots, n\}$ as follows:

$$s_i = \sum_{j=1}^{r} \sum_{\kappa=1}^{p} \beta_{\kappa}^{(j)} (e_i^{(j)})^{\kappa} \tag{1}$$

where p is the order of the considered nonlinearity, $e_i^{(j)}$ is the contribution on the i-th band of the j-th endmember and $\beta_{\kappa}^{(j)}$ is the κ-th order nonlinear coefficient for the j-th endmember.

The goal of nonlinear spectral unmixing is to evaluate each β term, in order to understand the nature of the endmember combination that delivers the given target pixel reflectance. In [12], the authors provide an unsupervised method to efficiently estimate the coefficients that drive the nonlinear combination by means of a linear system involving the original hyperspectral data and the endmembers' spectra delivered by an EEA.

The method in [12] requires to consider the H-representation of the skeleton of a polytope with n vertices $\underline{v} = [v_i]_{i=1,\ldots,n}$, where each vertex is identified by a string of n coordinates, i.e., $v_i \Leftrightarrow (v_{i_k})_{k=1,\ldots,n}$, $\forall i \in \{1, \ldots, n\}$, being $v_{i_k} = s_i$ if $k = i$, whereas $v_{i_k} = 0$ otherwise. Thus, by including the trigonometric function which relate two polytope vertices over each of the $m = \binom{n}{2}$ facet-defining half spaces in a linear system, the polytope representation of $\underline{s}$ can be decomposed into a set of linear equations. Specifically, it is possible to prove that (1) can be written as follows:

$$\underline{\underline{G}}\,\underline{\beta} = \underline{b} \tag{2}$$

where $\underline{\beta} = [\beta^{(j)}]_{j=1,\ldots,r}$, being $\beta^{(j)} = [\beta_{\kappa}^{(j)}]_{\kappa=1,\ldots,p}$. $\underline{\underline{G}} = [g_{k\lambda}]$ is a $m \times rp$ matrix, $k \in \{1, \ldots, m\}$ and $\lambda \in \{1, \ldots, rp\}$. k can be expressed as a function of two quantities η_t and ρ_t, $t \in \{1, \ldots, n-1\}$, $\eta_t \in \{1, \ldots, n-t\}$ and $\rho_t = \sum_{u=1}^{t-1} n - u$ if $t > 1$, whereas $\rho_t = 0$ if $t = 1$. Moreover, $\lambda = (z-1)p + \psi_p$, $z \in \{1, \ldots, r\}$ and $\psi_p \in \{1, \ldots, p\}$. Thus, each element $g_{k\lambda}$ can be defined as follows:

$$g_{k\lambda} = g_{(\rho_t+\eta_t),\lambda} = (e_t^{(z)})^{\psi_p} + \tan(\gamma_{(t,t+\eta_t)}) \cdot (e_{t+\eta_t}^{(z)})^{\psi_p} \tag{3}$$

where γ_{ml} is the angle s.t. $\tan(\gamma_{ml}) = s_m / s_l$. Finally, $b_k = b_{(\rho_t+\eta_t)} = 2s_t$. Therefore, it is possible to estimate $\underline{\beta}$ by left multiplying both the terms in (2) by the inverse of $\underline{\underline{G}}$ using the so-called thin QR decomposition [13].

2.2. Artificial neural network (ANN)

Although many neural network architectures exist, feed-fordward networks have been widely used in the context of mixed pixel decomposition in terms of nonlinear relationships [14, 8, 15]. In this work we adopt a multilayer perceptron (MLP) architecture which is easily adaptable to provide both fractional class-cover estimations and nonlinearity order estimations, due to its proved ability as a logistic regressor and also as a nonlinear classifier.

The MLP is composed of an input layer, two hidden layers and an output layer. The node count in the input layer is fixed to the spectral dimensionality of the data (number of spectral bands of the considered dataset). The number of output nodes depends on the application; if the network is used to unmix, the number of nodes equals the number of extracted endmembers while in the case of nonlinear order estimation it equals the maximum number of posible orders. In order to avoid over-fitting and improve generalization, we decided to use sufficiently large hidden layers in combination with regularization techniques (instead of early-stopping or cross-validation techniques) which involve the modification of the performance function embedding a term that consists of the mean of the sum of squares of the network weights and biases. Particularly, we use the Bayesian regulation backpropagation training algorithm, which updates the weight and bias according to Levenberg-Marquard optimization algorithm, which is used to estimate the Hessian matrix of the performance function. Finally, logistic activation functions are used in both hidden layers while we alternate between logistic and hyperbolic tangent in the output layer, depending on the application.

Apart from the difference in the activation function of the output layer, a main difference between ANN-based unmixing and ANN-based nonlinearity order estimation is related with the training and test set of samples. In the case of neural-based unmixing, we assume that there exist sufficient ground-truth information at fractional cover level and, therefore, we just provide the network with a sufficient random percentage of the available reference information for training, using the rest of the information for testing. In turn, if there is no sufficient reference information, the proposed approach may suffer from the well known Hughes effect [16]. However, if the ANN is used to estimate the nonlinearity order of an image, due to the lack of available reference information for real images we adopt an innovative approach where, from the endmembers extracted by an EEA, we generate synthetic nonlinear combinations of their spectral signatures using Eq. (1). Then, we use such nonlinear combinations to generate both training and test sets to be used during the ANN training stage. It should be noticed that we can generate infinite training and testing samples from an *a priori* estimated set of endmembers, being the range of possible nonlinearity orders the only needed parameter, thus reducing the impact of the curse of dimensionality. Further information about ANN parametrization will be shown in the next section.

3. EXPERIMENTAL RESULTS

We first tested the performance of the aforementioned methods over a target that has been artificially generated in [17]. Specifically, the

authors in [17] provide a good simulation of a crater obtained by modifying a martian regolith. This target shows a complex photometric behavior because of its digital elevation model (DEM) and the Hapke's model-based mixture of the composing minerals (i.e., basalt, palagonite and tephra). The target scene is composed by 186×174 pixels. 16 bands in a wavelength range from 400 nm to 1100nm have been considered. Fig. 2(a) shows the reflectance map of the aforementioned scene over the 16-th band. Further, the abundance maps of basalt, palagonite and tephra are reported in Fig. 2(b), (c) and (d), respectively.

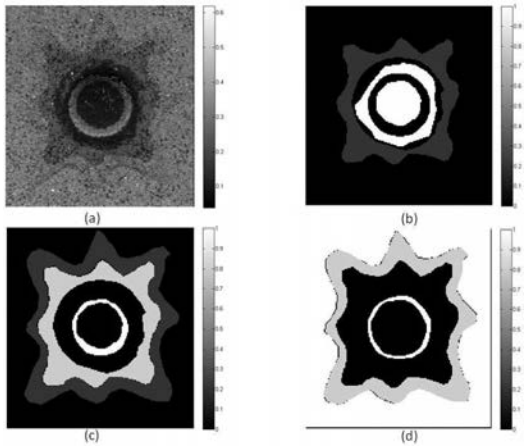

Fig. 2. (a) Original reflectance distribution in the crater scene on the 16-th band. Each endmember is distributed according to the reported abundance maps: basalt (b), palagonite (c) and tephra (d).

In [17], the authors deliver several methods to unmix the aforementioned image by deconvoluting the mixing process. These algorithms differ in the available quantitative information of the target they use to perform the unmixing process. Specifically, given the bidirectional reflectance image, they can consider conversion in single scattering albedo, information on incidence and emergence angles, material properties and surface macroscopic roughness in a pixel. On the other hand, POD is used to unmix the bidirectional reflectance image by considering the endmembers' reflectance spectra provided in [17]. It is worth noting that no other information but the target and the endmembers' reflectance spectra are available for POD.

We compared the unmixing performance by computing the mean absolute difference of the mineralogical fraction images (MFIs) [17] for each endmember. In order to obtain the abundance maps from polytope decomposition, we unmixed the reconstructed image by using a fully constrained least-squares unmixing (FCLSU) [18] approach, fed with the original endmembers' reflectance spectra. Then, we computed the percentage of mean absolute difference between calculated MFI and ideal MFI for each algorithm. We used FCLSU since the POD was not able to efficiently track the abundances over the crater scene on itself. Fig. 3 reports the aforesaid quantity for polytope decomposition with FCLSU (POD + FCLSU), artificial neural network (ANN), and those provided in [17]. The nonlinearity order p in POD has been set to 3. Apparently, POD delivers very poor performance in reconstructing the crater scene. One of the main reasons for this result lies in the mismatch between the Hapke's model and the polynomial approximation implied by POD method. Since POD is unable to efficiently track the non linearity induced by the bidirectional reflectance model, the reconstruction can be dramatically degraded. Moreover, it is worth to note that the linear estimation of the abundance maps from an image that has been not very efficiently nonlinearly reconstructed can further jeopardize the MFI evaluation as well. On the other hand, taking advantage of the perfect knowledge of the original MFIs to train the estimator, ANN is able to outperform all the other methods.

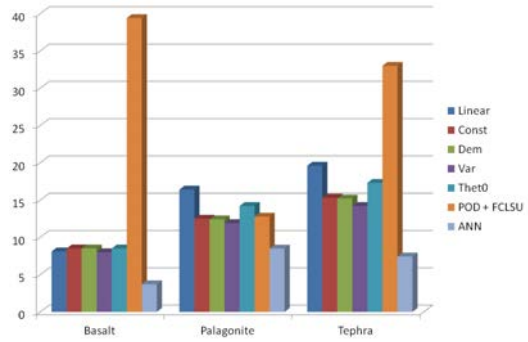

Fig. 3. Percentage of mean absolute difference of the mineralogical fraction images (MFIs) for each endmember in the crater scene. The considered methods are polytope decomposition followed by fully constrained least-squares unmixing approach (POD+FCLSU), artificial neural network (ANN), and those provided in [17].

We also tested the performance of the methods in Section 2 over a real image recorded over the Istanbul area by Hyperion in 2001. The scene is composed by 400×400 pixels. 198 calibrated bands in a wavelength range spanning from 426.82 nm to 2395.5 nm have been considered. We can summarize the reconstruction performance of the considered unmixing methods by means of the so-called reconstruction error (RE), which can be defined (for an image composed by $M \times N$ pixels over n bands) as:

$$RE = \sqrt{\frac{1}{MNn} \sum_{i=1}^{MN} ||\underline{s}_i - \underline{\hat{s}}_i||^2} \tag{4}$$

where $\underline{\hat{s}}_i$ is the reconstructed spectral signature of the i-th pixel.

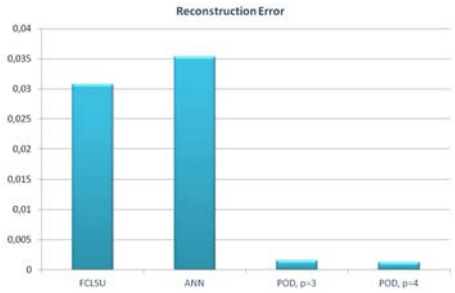

Fig. 4. Reconstruction error (RE) obtained over the Istanbul scene using fully constrained least-squares unmixing (FCLSU), artificial neural network (ANN) and polytope decomposition (POD) when the order of the considered nonlinearity p is set to 3 and 4. 10 endmembers have extracted using orthogonal subspace projection (OSP).

Fig. 4 reports the RE performance delivered by three unmixing methods: FCLSU, ANN and POD. These algorithms have been fed with the reflectance spectra of 10 endmembers that have been ex-

tracted by means of orthogonal subspace projection (OSP) [19]. Further, POD is performed when the nonlinearity order p is set to 3 and 4. Apparently, POD outperforms both the other methods. Specifically, POD reaches $RE = 1.2 \cdot 10^{-3}$ when $p = 4$, while ANN's reconstruction error is about 0.035. This behavior is the result of the lack of ground truth information at sub-pixel level over the Istanbul scene apart from the endmembers obtained by the EEA. Thus, ANN is not able to properly train its network in order to achieve a good approximation of the nonlinear mixing process.

Further, we tested the performance in terms of reconstruction error of the combined ANN-POD architecture shown in Fig. 1. Here, the endmembers of the Istanbul scene have been extracted using automatic target generation procedure (ATGP) algorithm [20], which provided the reflectance spectra of 5 endmembers. ANN estimates the maximum order of polynomial nonlinearity for every pixel in the scene. Then, this information is delivered to POD algorithm together with the endmembers' spectra. In this context, POD algorithm is performed over each pixel by setting the nonlinearity order p to the corresponding estimated order provided by ANN.

Fig. 5 shows the RE performance for the new ANN-POD architecture introduced in this work. Specifically, the blue solid line represents the RE achieved using ANN followed by POD as a function of the number of samples that have been used for training. The estimation of the nonlinearity order has been repeated 10 times for each case combining the results by majority voting. It is not surprising that the RE performance improves as the number of training samples increases. Moreover, the dashed lines identify the REs that have been achieved when only POD is used, setting the nonlinearity order p to 3 (green line), 4 (red line) and 5 (black line) for each pixel in the scene. Comparing these results to the RE curve we got from the combination of ANN and POD, we can see that the number of training samples plays a key-role in providing good reconstruction performance. In fact, the proposed framework outperforms POD when 4000 samples are used to train the ANN. Thus, apparently, the estimation of the nonlinearity order by ANN is delivering actual reconstruction results as the training is performed over a larger amount of pixels. It should be noticed that we synthetically generate the training samples, thus the availability of ground-truth information is not a problem.

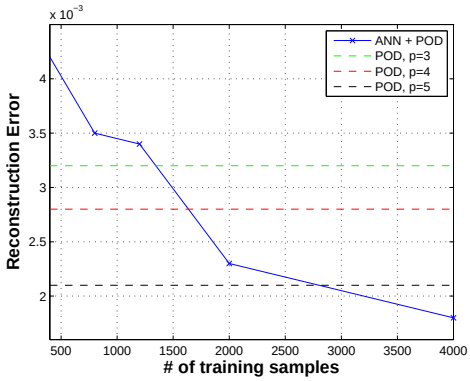

Fig. 5. Reconstruction error for the Istanbul scene as a function of the number of training samples that have been used by the ANN to estimate the nonlinearity order p of each pixel (blue solid line). The dashed green, red and black lines identify the RE that has been obtained using POD when p has been set for every pixel to 3, 4 and 5, respectively.

4. CONCLUSIONS AND FUTURE LINES

In this paper, we have developed a new method for nonlinear spectral unmixing which combines artificial neural networks (ANNs) and polytope decomposition (POD). The ANN is used to estimate the order of the nonlinearity involved in the problem, while POD is used to perform the actual unmixing. Our experimental results with both simulated and real hyperspectral data sets show promising results. Future work will focus on testing the proposed framework in different scenarios, in order to evaluate its capacity to provide effective solutions using limited or no prior information.

5. REFERENCES

[1] J. Bioucas-Dias, A. Plaza, N. Dobigeon, M. Parente, Q. Du, P. Gader, and J. Chanussot. Hyperspectral unmixing overview: Geometrical, statistical, and sparse regression-based approaches. *IEEE J. Sel. Topics Appl. Earth Observ. and Remote Sens.*, 5(2):354–379, 2012.

[2] N. Keshava and J.F. Mustard. Spectral unmixing. *IEEE Signal Processing Mag.*, 19(1):44–57, 2002.

[3] W.-K. Ma, J.M. Bioucas-Dias, Tsung-Han Chan, N. Gillis, P. Gader, A.J. Plaza, A. Ambikapathi, and Chong-Yung Chi. A signal processing perspective on hyperspectral unmixing: Insights from remote sensing. *IEEE Signal Processing Magazine*, 31(1):67–81, Jan 2014.

[4] A. Plaza, P. Martinez, R. Perez, and J. Plaza. A quantitative and comparative analysis of endmember extraction algorithms from hyperspectral data. *IEEE Trans. Geosci. and Remote Sens.*, 42(3):650–663, 2004.

[5] A. Plaza, G. Martin, J. Plaza, M. Zortea, and S. Sánchez. Recent developments in spectral unmixing and endmember extraction. In S. Prasad, L. M. Bruce, and J. Chanussot, editors, *Optical Remote Sensing*, chapter 12, pages 235–267. Springer-Verlag, Berlin, Germany, 2011.

[6] B. Hapke. *Theory of Reflectance and Emittance Spectroscopy*. Cambridge University Press, 1993.

[7] J. Broadwater, A. Banerjee, and P. Burlina. Kernel methods for unmixing hyperspectral imagery. In L. Bruce S. Prasad and Eds. J. Chanussot, editors, *Optical Remote Sensing Advances in Signal Processing and Exploitation*, pages 247–269. Springer, 2011.

[8] J. Plaza and A. Plaza. Spectral mixture analysis of hyperspectral scenes using intelligently selected training samples. *IEEE Geosci. Remote Sens. Lett.*, 7:371–375, 2010.

[9] J. Plaza, A. Plaza, R. Perez, and P. Martinez. On the use of small training sets for neural network-based characterization of mixed pixels in remotely sensed hyperspectral images. *Pattern Recogn..*, 42:3032–3045, 2009.

[10] Yoann Altmann, Abderrahim Halimi, Nicolas Dobigeon, and Jean-Yves Tourneret. Supervised nonlinear spectral unmixing using a post-nonlinear mixing model for hyperspectral imagery. *IEEE Trans. Image Process.*, 21(6):3017–3025, 2012.

[11] R. Heylen and P. Scheunders. Calculation of geodesic distances in nonlinear mixing models: Application to the generalized bilinear model. *IEEE Geosci. Remote Sens. Lett.*, 9(4):644–648, 2012.

[12] A. Marinoni and P. Gamba. Non-linear hyperspectral unmixing by polytope decomposition. In *Proc. WHISPERS*, Lausanne, Switzerland, June 2014.

[13] G. H. Golub and C. F. Van Loan. *Matrix computations*. Baltimore, MD: The Johns Hopkins University Press, 3nd edition, 1996.

[14] W. Liu and E. Y. Wu. Comparison of nonlinear mixture models: sub-pixel classification. *Remote Sensing of Envirnment*, 94:145–154, 2005.

[15] J. Plaza, R. Perez, P. Martinez, and A. Plaza. Joint linear/nonlinear spectral unmixing of hyperspectral image data. In *Proc. of IEEE International Geoscience and Remote Sensing Symposium*, Barcelona, Spain, July 2007.

[16] G. Hughes. On the mean accuracy of statistical pattern recognizers. *IEEE Trans. on Inf. Theory*, 14(1):55–63, January 1968.

[17] A.M. Cord, P.C. Pinet, Y. Daydou, and S.D. Chevrel. Experimental determination of the surface photometric contribution in the spectral reflectance deconvolution processes for a simulated martian crater-like regolitic target. *Icarus*, 175(1):78–95, August 2004.

[18] D. Heinz and C.-I Chang. Fully constrained least squares linear mixture analysis for material quantification in hyperspectral imagery. *IEEE Trans. Geosci. and Remote Sens.*, 39:529–545, 2001.

[19] J. C. Harsanyi and C.-I Chang. Hyperspectral image classification and dimensionality reduction: An orthogonal subspace projection. *IEEE Trans. Geosci. and Remote Sens.*, 32(4):779–785, 1994.

[20] H. Ren and C.-I Chang. Automatic spectral target recognition in hyperspectral imagery. *IEEE Trans. Aerospace and Electron. Syst.*, 39(4):1232–1249, 2003.